nature plants

ARTICLES

https://doi.org/10.1038/s41477-021-00976-0

Quantitative imaging of RNA polymerase II activity in plants reveals the single-cell basis of tissue-wide transcriptional dynamics

Simon Alamos[1], Armando Reimer[2], Krishna K. Niyogi[1,3,4] ✉ and Hernan G. Garcia[2,5,6,7] ✉

The responses of plants to their environment are often dependent on the spatiotemporal dynamics of transcriptional regulation. While live-imaging tools have been used extensively to quantitatively capture rapid transcriptional dynamics in living animal cells, the lack of implementation of these technologies in plants has limited concomitant quantitative studies in this kingdom. Here, we applied the PP7 and MS2 RNA-labelling technologies for the quantitative imaging of RNA polymerase II activity dynamics in single cells of living plants as they respond to experimental treatments. Using this technology, we counted nascent RNA transcripts in real time in *Nicotiana benthamiana* (tobacco) and *Arabidopsis thaliana*. Examination of heat shock reporters revealed that plant tissues respond to external signals by modulating the proportion of cells that switch from an undetectable basal state to a high-transcription state, instead of modulating the rate of transcription across all cells in a graded fashion. This switch-like behaviour, combined with cell-to-cell variability in transcription rate, results in mRNA production variability spanning three orders of magnitude. We determined that cellular heterogeneity stems mainly from stochasticity intrinsic to individual alleles instead of variability in cellular composition. Together, our results demonstrate that it is now possible to quantitatively study the dynamics of transcriptional programs in single cells of living plants.

Plant growth and development depends on rapid and sensitive signalling networks that monitor environmental fluctuations and transduce this information into transcriptional changes that lead to physiological adaptation. Gene regulation in plants can be extremely rapid, with changes in mRNA abundance detectable in minutes or less, for example in response to modulations in light intensity[1], light quality[2], nutrient concentration[3] or temperature[4].

A first step towards understanding how plant transcriptional programs unfold in time and space is to quantify gene activity in individual living cells as they respond to external stimuli. Protein reporters have been used in plants to measure the dynamics of single-cell gene activity in live tissues[5] over hours to days. However, fluorescent proteins mature at timescales that are long (over 30 min) compared with the rates that characterize stress-responsive transcription[6] (approximately 1 min), particularly at moderate temperatures such as those typically encountered by plants[7]. In addition, protein reporter signals convolve processes such as transcription, RNA processing, RNA transport, translation and protein degradation, often making it challenging to precisely identify where and how regulatory control is being applied along the central dogma.

Over the past few years, our understanding of transcriptional regulation in animals has been transformed by techniques that have made it possible to quantify transcriptional activity in single cells of living fruit fly embryos[8,9], in the nematode *Caenorhabditis elegans*[10] and in adult mouse tissue[11]. these techniques involve fluorescently labelling nascent RNA by tagging genes of interest with RNA aptamers such as MS2 or PP7 that recruit fluorescent proteins to transcriptional loci, revealing real-time transcriptional activity at the single-cell level. However, research into the equally diverse and important gene-regulatory aspects of plant development and physiology has remained relatively isolated from these technological breakthroughs. Indeed, MS2 and other similar approaches based on RNA-binding proteins have been used in plants to visualize the movement and localization of cytoplasmic RNAs[12–14], but not their nuclear transcriptional dynamics.

Here we bridged this technological gap by developing and implementing the PP7 and MS2 technologies for labelling nascent RNA in *A. thaliana* and *N. benthamiana* (tobacco). Using state-of-the-art quantitative imaging, we counted the absolute number of elongating RNA polymerase II (RNAP) molecules at individual genes and measured how this number is regulated dynamically in response to heat stress. We used this stress response in leaves as a model to determine how tissue-level patterns of mRNA accumulation arise from the dynamical transcriptional behaviour of individual cells. Using this technology, we also uncovered previously unmeasurable modes of gene regulation in plants by which tissues respond to external signals by modulating the fraction of cells engaged in transcription, but leave the single-cell transcription rate unchanged. Further, we determined how these regulatory layers give rise to high cell-to-cell variability—spanning three orders of magnitude—in mRNA production. The single-locus resolution afforded by PP7 and MS2 made it possible to characterize the sources of this cell-to-cell variability, revealing that stochastic processes intrinsic to individual alleles are the main contributors to this variability, independent of differences in cellular composition. Together, these results highlight the potential of live-imaging techniques for uncovering and quantitatively describing regulatory processes with spatiotemporal resolutions that cannot be achieved with methods such as traditional

[1]Department of Plant and Microbial Biology, University of California Berkeley, Berkeley, CA, USA. [2]Biophysics Graduate Group, University of California Berkeley, Berkeley, CA, USA. [3]Howard Hughes Medical Institute, University of California Berkeley, Berkeley, CA, USA. [4]Molecular Biophysics and Integrated Bioimaging Division, Lawrence Berkeley National Laboratory, Berkeley, CA, USA. [5]Department of Molecular and Cell Biology, University of California Berkeley, Berkeley, CA, USA. [6]Department of Physics, University of California Berkeley, Berkeley, CA, USA. [7]Institute for Quantitative Biosciences-QB3, University of California Berkeley, Berkeley, CA, USA. ✉e-mail: niyogi@berkeley.edu; hggarcia@berkeley.edu

protein reporters or single-cell RNA sequencing. We envision that this approach will open new avenues of inquiry in plant physiology, and cell and developmental biology.

Results

Establishment of the PP7 and MS2 systems for single-cell live imaging of transcription in plants. To quantitatively measure transcriptional dynamics in tobacco and *Arabidopsis*, we implemented an mRNA fluorescent-tagging approach—previously used in cells in culture[15], *Drosophila melanogaster* embryos[8,9], the mouse brain[11] and *C. elegans*[10]—in which the gene of interest is tagged with tandem repeats of the PP7 DNA sequence that, when transcribed, form RNA stem–loops (Fig. 1a). The PP7 loop RNA is bound by the PP7 bacteriophage coat protein (PCP)[16] expressed under a ubiquitous promoter. Fusing PCP to a fluorescent protein results in the fluorescent labelling of nascent RNA molecules. By virtue of the relatively slow movement of genomic loci in the nucleus and the accumulation of fluorophores in the diffraction-limited volume of the gene, sites of active transcription appear as bright fluorescent puncta over the background of nuclear PCP fluorescence in a laser-scanning confocal microscope (Fig. 1a). The fluorescence intensity of these spots reports on the number of RNAP molecules actively transcribing the gene at any given time[9] and is proportional to the instantaneous rate of transcription[17].

To optimize this imaging strategy for plants, we generated two classes of constructs (Fig. 1b): first, coat protein constructs that fuse PCP to a fluorescent protein such as green fluorescent protein (GFP) under a constitutive and ubiquitously expressed *Arabidopsis* promoter, and second, reporter constructs that contain a neutral DNA sequence consisting of a firefly luciferase-β-glucoronidase fusion with 24 PP7 stem loop repeats inserted in the 5′ end of this gene, under the control of the promoter of interest. To aid in the automated segmentation of nuclei, reporter constructs also contain a nuclear label consisting of the mScarlet red fluorescent protein[18] fused to the *Arabidopsis* histone 2B coding region driven by the UBQ10 ubiquitous and constitutive promoter. These two constructs confer resistance to different antibiotics, allowing sequential and combinatorial transformation into plants.

We tested this system in tobacco by simultaneously infiltrating leaves with two *Agrobacterium* strains, one strain carrying a PCP–GFP plasmid and a second strain carrying a reporter plasmid lacking a functional promoter, yielding homogeneous GFP nuclear and cytoplasmic fluorescence (Fig. 1c, top left). When the strong and constitutive 35S promoter was used to drive the reporter construct, nuclear GFP puncta became visible (Fig. 1c, top right). These results suggest that spots correspond to sites of active transcription and are not an artefact of PCP–GFP aggregation in the nucleus. Analogous results were obtained in stably transformed transgenic *Arabidopsis* plants (Fig. 1c, bottom).

We next sought to confirm that spot fluorescence constitutes a dynamical readout of transcriptional activity. To this end, we investigated whether spot fluorescence dynamics in tobacco qualitatively recapitulate previous observations performed on the same promoters in *Arabidopsis* with orthogonal techniques. This comparison is made possible by the strong conservation of transcriptional regulation in plants, in particular the heat shock response[19]. We measured the transcriptional activity of two well-known constitutive and heat shock-inducible *Arabidopsis* genes (*GAPC2* and *HSP70*, respectively[20,21]) before and during a heat shock treatment. GAPC2–PP7 expression was detectable at 25 °C (Fig. 1d, top left and Supplementary Video 1). The presence of multiple spots per nucleus is probably due to multiple transgene transfer events; the number of spots did not change with treatment (Fig. 1d, bottom left and Supplementary Fig. 1). Further, the fluorescence of these spots over time did not change upon heat shock (Fig. 1e and Supplementary Fig. 1), in accordance with the constitutive expression of *GAPC2* in *Arabidopsis*[20]. Consistent with the heat shock inducibility of the *HSP70* gene in *Arabidopsis*[21], HSP70–PP7 transcription was hardly detectable at 25 °C in tobacco (Fig. 1d, top right and Supplementary Fig. 1). However, upon increasing the temperature to 39 °C, multiple fluorescent puncta rapidly appeared (Fig. 1d, bottom right, Supplementary Fig. 1 and Supplementary Video 2), and their fluorescence increased with time (Fig. 1e and Supplementary Fig. 1). A reporter construct where the PP7 cassette is inserted in an intron of *Arabidopsis HSP70* fused in its C-terminus to mCherry, confirmed that appearance of transcriptional spots is associated with the accumulation of the gene products (Supplementary Fig. 2). Thus, we conclude that the PP7 system reliably recapitulates previous qualitative knowledge of transcriptional dynamics in plants.

Simultaneously tagging multiple mRNA species or multiple locations of the same mRNA species with different fluorescent proteins has revealed regulatory and physical interactions between loci and uncovered the regulation of distinct steps of the transcription cycle in cells in culture and animals[22–24]. To enable such multiplexing in plants, we also implemented the MS2 system, which is analogous and orthogonal to the PP7 system. Here, MS2 loops are specifically recognized by an MS2 coat protein (MCP)[25]. We tested the MS2 system in tobacco and obtained results comparable to those obtained for PP7 (Supplementary Fig. 3), allowing us to track the expression dynamics of two transgenes in a single cell (Fig. 1f).

Quantitative characterization of the PP7 system in *Arabidopsis*. To study transcriptional regulation at the single-cell level in populations of genetically identical leaf cells, we next generated stably transformed lines of *Arabidopsis* carrying PCP–GFP and a PP7 reporter construct driven by the promoter of the stress-inducible *HSP101* gene. A line carrying a single reporter locus (hereafter referred to as HSP101-PP7-1) was used for the following experiments unless stated otherwise (details are in Methods, 'Generation of transgenic *Arabidopsis* lines').

A key step towards establishing PP7 as a reporter of single-cell transcriptional activity in *Arabidopsis* is to demonstrate that the observed spot fluorescence dynamics quantitatively recapitulate this activity. We therefore sought to cross-validate PP7 measurements with quantitative PCR with reverse transcription (RT–qPCR) quantifications of reporter transgene mRNA abundance in our stably transformed *Arabidopsis* plants. The *HSP101* mRNA is hardly detectable across vegetative tissues under standard growth conditions[26] and accumulates to high levels as quickly as 2 min following treatments inducing cytosolic protein misfolding such as heat shock[4]. As previous experiments have shown that, upon induction, *HSP101* is expressed uniformly throughout plant tissues[27], we compared the average transcriptional activity of a few hundred leaf cells obtained by microscopy with that of the whole plant in bulk reported by RT–qPCR.

As expected, we did not detect actively transcribing cells in HSP101-PP7-1 plants imaged for 1 h at room temperature (Supplementary Fig. 4), but shifting the microscope stage from 22 °C to 39 °C resulted in the rapid appearance of transcription spots (Fig. 2a and Supplementary Video 3). To compare the instantaneous metric of transcriptional activity reported by spot fluorescence with the number of accumulated reporter mRNA molecules captured by RT–qPCR, we converted spot fluorescence to number of produced mRNA molecules by integrating the fluorescence of all spots in the field of view over time[9] (Supplementary Fig. 5 and associated calculations in Supplementary Section 1.1).

Controls for GFP photobleaching ruled out the possibility that we underestimated the produced mRNA calculated by microscopy (Supplementary Fig. 6). Finally, we measured HSP101 reporter mRNA abundance by RT–qPCR using whole plants treated with heat shock (Methods, 'Heat shock treatments'). These measurements were strongly correlated with each other ($R^2 = 0.98$; Fig. 2b),

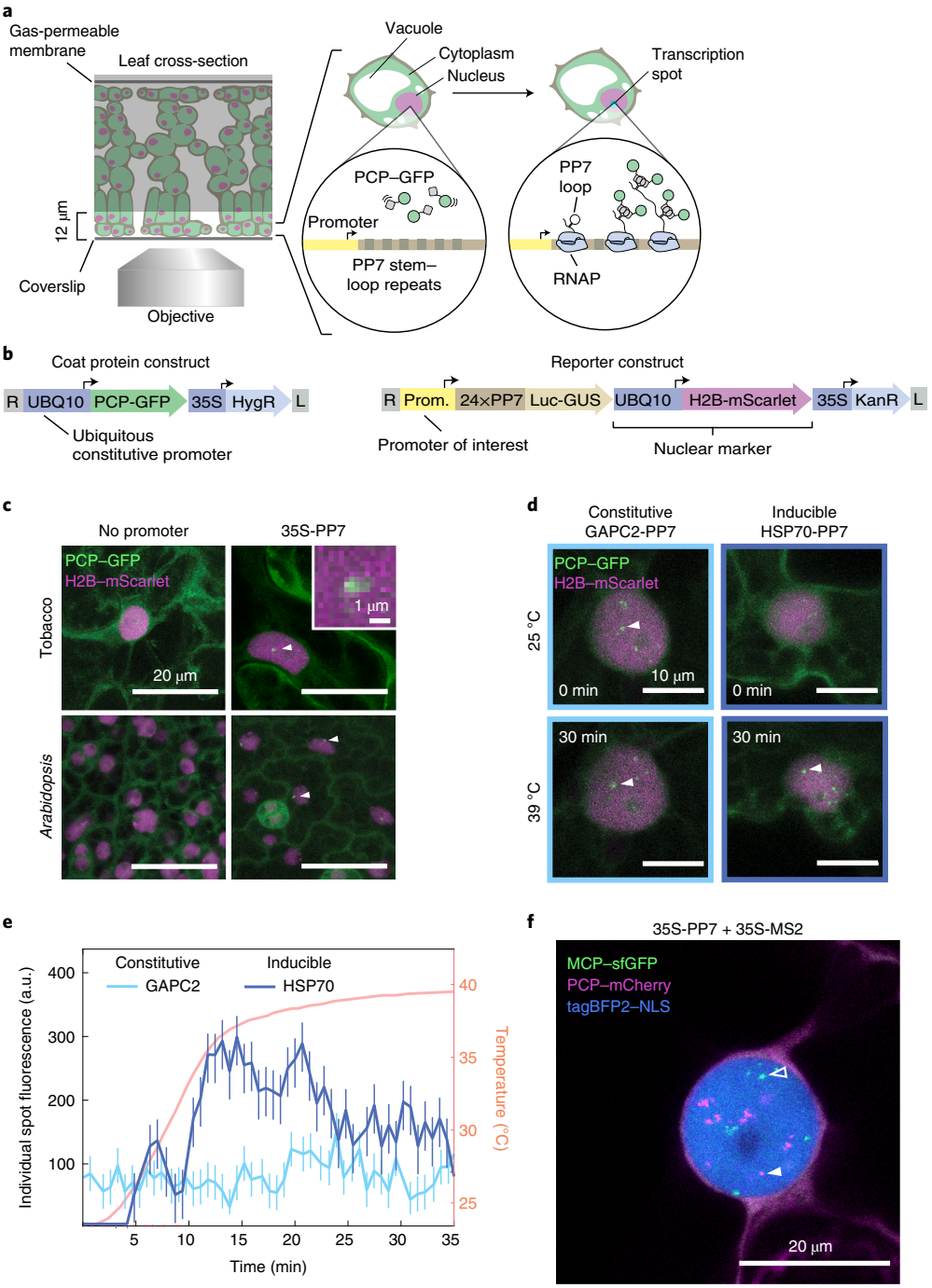

Fig. 1 | Fluorescence labelling of nascent RNA in tobacco and *Arabidopsis* reveals single-cell transcriptional dynamics in real time. a, Schematic of the live-imaging experimental setup in leaves and diagram of the PP7 RNA-labelling system. **b**, Schematic of the constructs used in this study. UBQ10, *Arabidopsis* ubiquitin 10 promoter; 35S, CaMV 35S promoter; HygR, hygromycin resistance; Luc-GUS, firefly luciferase-β-glucoronidase fusion; H2B, *Arabidopsis* histone 2B coding sequence; KanR, kanamycin resistance; L, T-DNA left border; R, T-DNA right border. **c**, Maximum projection of snapshots of cells expressing PCP–GFP and the reporter construct with or without the constitutive 35S promoter driving expression of the PP7-tagged Luc-GUS gene. White arrowheads indicate nuclear fluorescent puncta corresponding to transcription spots. Inset: magnification of PP7 fluorescence. **d**, Maximum projection snapshots of tobacco cells expressing PCP–GFP and reporter constructs driven by the promoters of the *Arabidopsis GAPC2* and *HSP70* genes. Time under heat shock is indicated. White arrowheads indicate the fluorescent spots quantified in **e**. **e**, Fluorescence time traces of single nuclear GFP puncta in tobacco leaf epidermis cells expressing PCP–GFP and reporter constructs driven by the promoters of the *Arabidopsis GAPC2* and *HSP70* genes. Each blue line corresponds to a single spot tracked over time. The orange line corresponds to the temperature experienced by the sample and is plotted on the right *y*-axis. Before spot detection, spots are assigned a fluorescence value of zero. Error bars represent the uncertainty in the spot fluorescence extraction (Methods, 'Spot fluorescence and tracking'). **f**, Maximum projection snapshot of tobacco leaf epidermal cell expressing PCP–mCherry, MCP–GFP, H2B–tagBFP2 and two reporter constructs driven by the 35S promoter and tagged with PP7 (magenta) or MS2 (green). Open and closed arrowheads indicate MCP-tagged and PCP-tagged nascent RNAs, respectively (see also Supplementary Fig. 3).

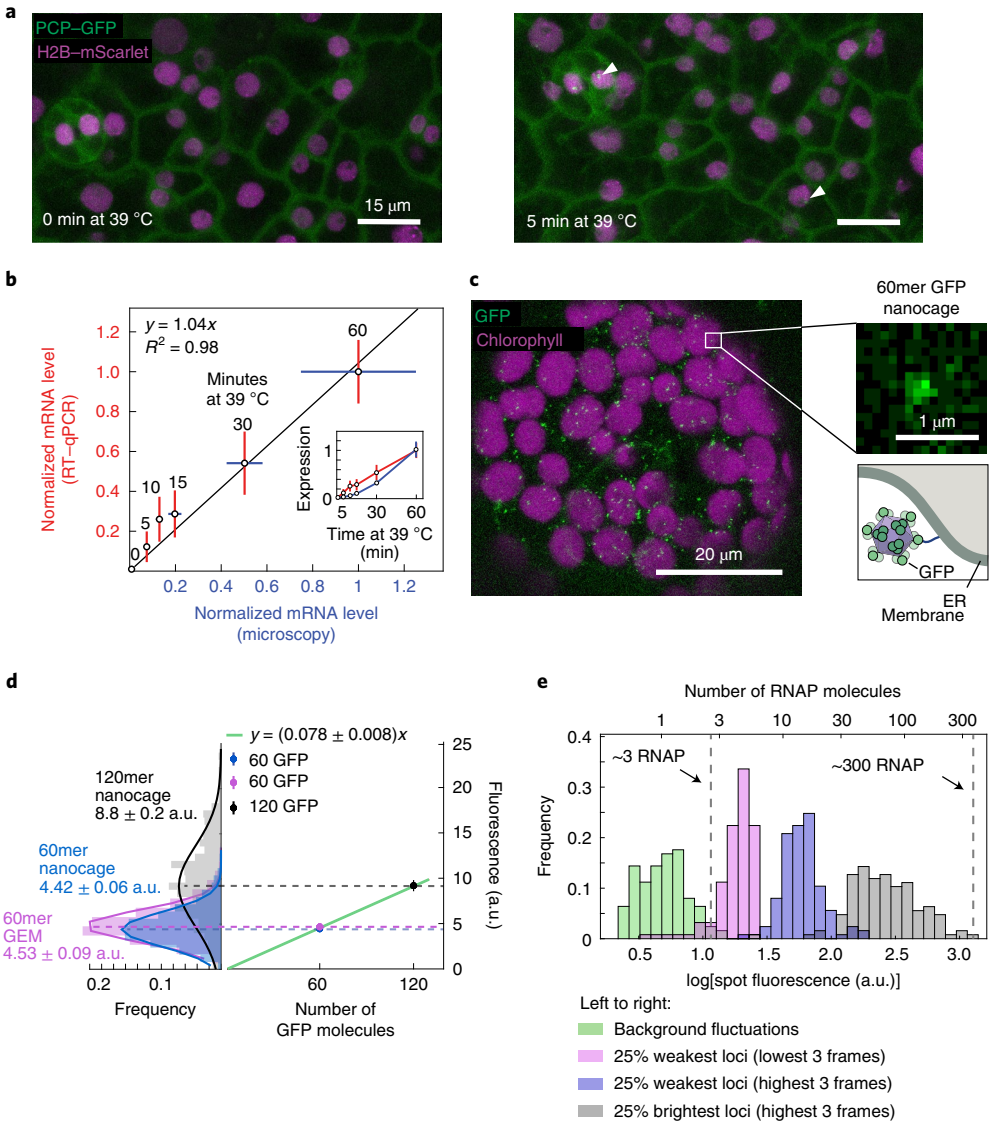

Fig. 2 | Cross validation, absolute calibration and sensitivity of the PP7 reporter system. a, Maximum fluorescence projections of leaf epidermal tissue of an *Arabidopsis* line stably transformed with PCP–GFP and a reporter construct driven by the HSP101 promoter under heat shock. Time stamps indicate time under heat shock. Arrowheads point to transcription spots. **b**, Comparison between total mRNA produced as reported by RT–qPCR (red) and by PCP–GFP (blue) under microscopy. PCP–GFP data are mean ± s.e.m. of $n = 8$ biological replicates; RT–qPCR data are mean ± s.e.m. of $n = 3$ biological replicates. Data are normalized to each corresponding signal at 60 min. The solid black line shows a linear fit to the data going through the origin. The inset shows the normalized mean ± s.e.m. of expression level as a function of time for RT–qPCR (red) and microscopy (blue). **c**, Maximum fluorescence projection of a tobacco mesophyll cell expressing a construct encoding a 60-GFP nanocage tethered to the outer side of the endoplasmic reticulum (ER) membrane. **d**, Left: absolute calibration of GFP fluorescence. Histograms and Gaussian fit of fluorescence values of individual spots for the 60-GFP nanocage (blue), 60-GFP GEM (magenta) and 120-GFP nanocage (black) transiently expressed in tobacco leaves. The mean of each distribution is shown next to each histogram. As expected, the means are related by a factor of two. Data are mean ± s.e.m. Right: fluorescence of the nanocages and GEM (mean ± s.e.m.) as a function of number of GFP molecules per structure ($n = 500$ (60mer nanocage), 137 (120mer nanocage) and 1,037 (60mer GEM) spots). The green line is a linear fit passing through the origin, revealing a calibration factor of 0.078 ± 0.008 a.u. per GFP molecule (error reporting on the 95% confidence interval of the fit) (Methods, 'Absolute calibration using nanocages'). **e**, Histograms of the calibrated number of transcribing RNAP molecules in the weakest three frames of the weakest 25% of HSP101-PP7 fluorescence time traces (magenta) and their associated fluorescence background fluctuations (green) from all spot fluorescence time traces across all 8 replicates from **b**. The point where the distributions overlap, at 3 RNAP molecules (vertical dashed line), can be considered the detection threshold. Also shown are the brightest 3 frames of the weakest 25% of all time traces (blue) and the brightest 3 frames of the strongest 25% of spot fluorescence time traces (grey).

confirming that spot fluorescence directly reports on the rate of mRNA production. This conclusion held regardless of the magnitude of the mRNA degradation rate (Supplementary Fig. 10 and associated calculations in Supplementary Section 1.1).

While our measurements so far have shown that PP7 fluorescence is proportional to the number of actively transcribing RNAP molecules, this fluorescence does not, by itself, report on the absolute number of RNAP molecules. Expressing measurements in terms of absolute number of active RNAP molecules instead of arbitrary fluorescence units is necessary for directly comparing data across microscopy setups and laboratories, and for integration with other quantitative measurements and theoretical models[9,17]. To turn the PP7 system into such

a precision tool, we calibrated its arbitrary fluorescence units to report on the number of RNAP molecules transcribing the reporter. We followed a recently established approach to measure the fluorescence of individual GFP molecules arranged in 60meric nanocages in vitro[28] and in vivo[29]. We fused GFP to a monomer that forms these 60meric nanocages and expressed it in tobacco leaves (Fig. 2c) to obtain a distribution of fluorescence intensity values for the resulting GFP punctae (Fig. 2d, left and Supplementary Fig. 8). Fusing two GFP molecules to each nanocage monomer yielded a fluorescence distribution of nanocages containing 120 GFP molecules (Fig. 2d, left). To further validate this approach we imaged a genetically encoded multimeric nanoparticle (GEM) containing 60-GFP-tagged monomers[30]. A linear fit of the means of these distributions passing through the origin shows that the mean fluorescence of the 120-GFP nanocage is almost exactly twice that of the 60-GFP nanocage and the 60-GFP GEM (Fig. 2d, right), confirming the validity of this approach. The slope of this fit is an estimate of the average number of arbitrary units of fluorescence corresponding to a single GFP molecule in our microscopy setup, making it possible to report PP7 measurements in absolute units.

Our absolute calibration also provided the opportunity to determine the limits of applicability of the PP7 technology. Specifically, there is a minimum number of actively transcribing RNAP molecules below which no reliable detection is possible. Figure 2e compares histograms of the calibrated number of RNAP molecules in the weakest detectable spots across all spots from all replicates from Fig. 1f and their corresponding fluctuations in background fluorescence. This calibration is based on the assumption that each PP7 loop is bound by two PCP–GFP molecules and each fully loaded RNAP carries 24 PP7 loops (details in Supplementary Section 1.2). Consistent with previous measurements[9,17], these background and signal histograms overlap at approximately 3 RNAP molecules, marking the level at which PP7 fluorescent spots become undetectable (Supplementary Fig. 9). An alternative way to view this detection limit is to consider the minimum detectable rate of transcription initiation. Given an elongation rate[31] of 1.5 kbp min^{-1} and the average unspliced transcript length[32] in *Arabidopsis* of about 2.5 kbp, a RNAP molecule takes about 2 min to transcribe an average *Arabidopsis* gene. Thus, to ensure at least 3 RNAP molecules on the gene and signal detectability at any time point, transcription needs to initiate at a minimum rate of 1.5 RNAP min^{-1}.

It is also informative to determine the dynamic range of our measurements in terms of the number of actively transcribing RNAP molecules. Given a footprint of an elongating RNAP molecule[33] of approximately 40 bp, an average *Arabidopsis* gene can accommodate a maximum of 2.5 kbp/40 bp ≈ 60 RNAP molecules (or a maximum density of 25 RNAP molecules per kbp), well above the minimum 3 RNAP molecules that constitute our detection limit. The strongest transcribing loci in our HSP101-PP7 experiment have a fluorescence of ≈ 1,000 fluorescence arbitrary units (a.u.), corresponding to ≈ 300 RNAP molecules (Fig. 2e). According to our quantitative PCR (qPCR) analysis (Supplementary Fig. 10 and Supplementary Section 1.3), the insertion locus of line HSP101-PP7-1 contains two copies of the reporter construct. Since our reporter has a length of approximately 4.9 kbp, the strongest loci have an RNAP density of about 30 RNAP molecules per kbp, showing that they are probably transcribing at the maximum possible rate.

Uncovering single-cell transcriptional responses to heat shock. While static snapshots of tissues have provided profound lessons about the spatial control of transcription in both animals and plants[34], these approaches have not revealed how single-cell transcriptional dynamics dictate the temporal modulation of gene-expression patterns. We sought to bridge this gap between single-cell and tissue-wide transcriptional dynamics by tracking individual nuclei and measuring the fluorescence of their corresponding transcription spot over time. To expand our range of inquiry, we generated two additional reporter lines under the control of a second heat shock-inducible promoter (HsfA2-PP7) (Supplementary Video 4) or of a constitutive promoter (EF-Tu-PP7) (Supplementary Video 5). To simplify our experiments, we focused on cells containing at most one spot per nucleus. We achieved this by imaging cells close to the base of the leaf which, according to their nuclear volume (Supplementary Fig. 11) and developmental stage, should be predominantly diploid[35,36]. Consequently, young epidermis cells in hemizygous *Arabidopsis* derived from the first generation of single-insertion transgenic plants (that is, T2 individuals) contained at most one spot per nucleus (Supplementary Fig. 12 and Methods, 'Microscopy setup and image acquisition').

A striking feature of the single-cell response is the existence of a reproducible fraction of nuclei that does not show detectable expression of the reporter transgene throughout the experiment in all three assayed promoters, which we define as transcriptionally refractory cells (Fig. 3a and Supplementary Fig. 13). The presence of these transcriptionally refractory cells was surprising given that endogenous *HSP101* and *HsfA2* are strongly induced and are necessary to survive heat stress in a dose-dependent manner[37,38]. Similarly, as a highly expressed constitutive gene, the EF-Tu promoter would also be expected to drive transcription in every cell. Yet this constitutive transgene also presents a substantial fraction of refractory cells (Fig. 3a, right). Such refractory cells have also been identified in live-imaging studies of the early development of the fruit fly[9,17] and in in vitro cultures of animal cells[39].

To confirm that the presence of refractory cells was not an artefact of our construct or of the PP7 technology, we examined a transgenic plant containing a HSP101–GFP fusion driven by the HSP101 promoter that fully complements the heat-susceptibility phenotype of a *hsp101* knockout[40]. Treatment of HSP101-GFP plants with the conditions used in our PP7 experiments revealed the presence of two types of cells: cells whose fluorescence was close to that of untreated cells and highly induced cells (Supplementary Fig. 14). These low-fluorescence cells, which can be located right next to highly expressing ones, support the existence of transcriptionally refractory cells and the ability of the PP7 technology to detect them.

This cellular heterogeneity in the response could arise from uneven heating across the field of view, however, a gradient of temperature with biologically relevant scales is unlikely to arise at a microscopic level (Methods, 'Heat shock treatments'). Consistent with this, we found that the spatial distribution of actively transcribing cells can be well described by a random distribution (Supplementary Fig. 15).

Within responsive nuclei, we also found substantial heterogeneity in the instantaneous number of actively transcribing RNAP molecules. For example, at any given time, not all responsive nuclei harboured fluorescent spots; the fraction of active nuclei is modulated in response to heat shock, but remains constant for the constitutive promoter (Fig. 3b). In addition, individual spots do not turn on synchronously and present periods of high transcriptional activity interspersed by periods of low to no detectable activity (Fig. 3c and Supplementary Figs. 16–18). This single-cell behaviour is consistent with the presence of transcriptional bursts, which have been identified across organisms and are believed to emerge from the intrinsically stochastic nature of the biochemical process of transcription[41]. The only plant gene—to our knowledge—previously probed in such detail lacked such bursts[42].

Finally, to demonstrate the applicability of this technique to other plant tissues, we imaged EF-Tu-PP7 and HsfA2-PP7 in *Arabidopsis* roots. The rapid rate of cell division in roots allowed us to capture the halting of transcription during mitosis[43] (Supplementary Fig. 19a–c). In addition, consistent with its behaviour in leaves, HsfA2 was expressed in only a fraction of nuclei at any given time (Supplementary Fig. 19d,e).

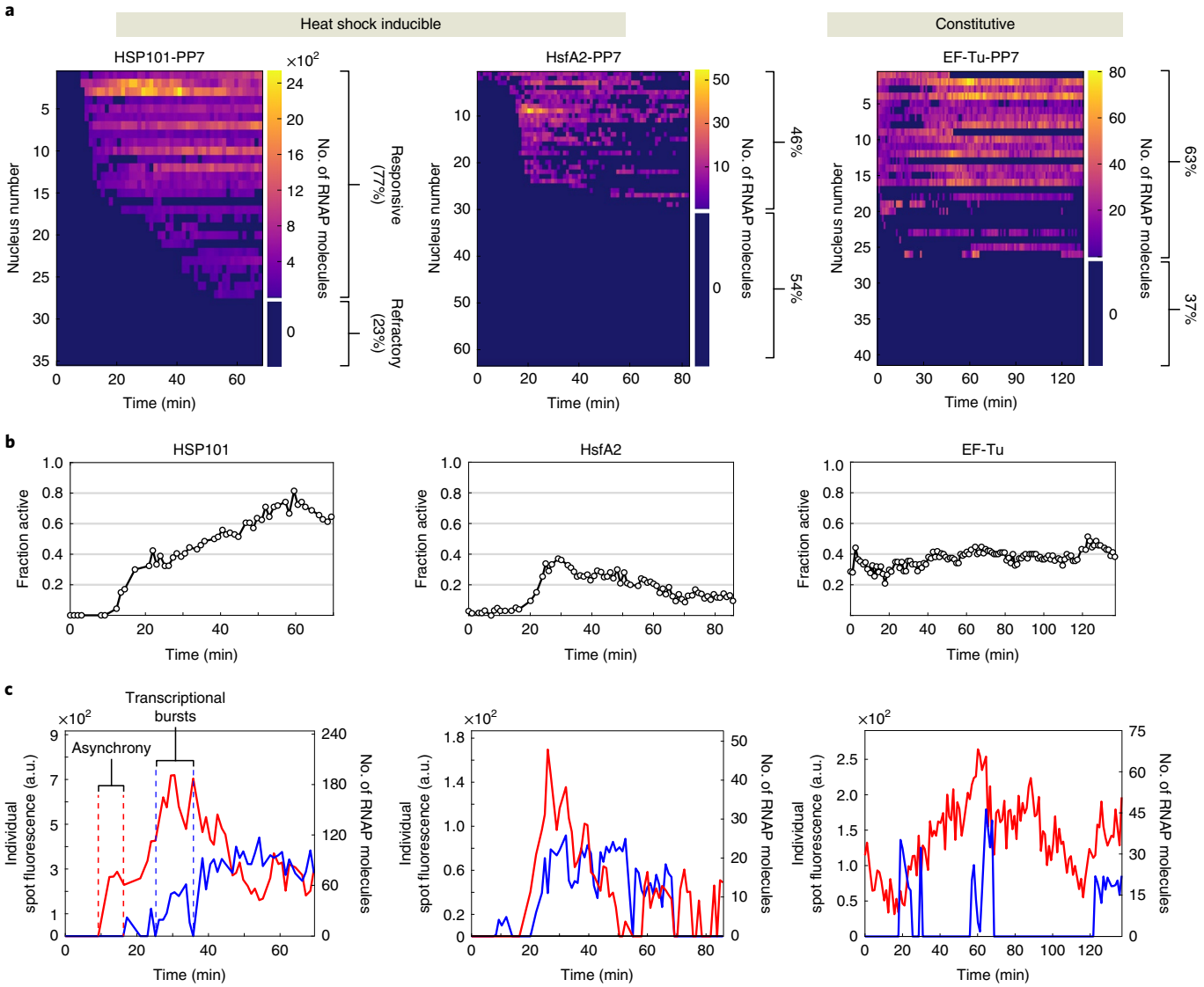

Fig. 3 | Single-cell control of transcriptional activity in response to heat shock in *Arabidopsis*. a, Heat maps of spot fluorescence in all nuclei (rows) over time (columns) across the the field of view in HSP101-PP7-1, HsfA2-PP7-1 and EF-Tu-PP7-1 plants. Dark blue represents the absence of detectable signal. The size of the colour bar on the right of each heat map shows the proportion of nuclei that exhibited activity in at least one frame during the experiment (>68 min) to refractory cells that presented no spots. **b**, Instantaneous fraction of actively transcribing nuclei measured as the number of nuclei with spots divided by the total number of nuclei in the field of view. **c**, Fluorescence time traces of two representative transcription spots in the same field of view shown in red and blue. Upon induction, transcriptional onset can occur asynchronously and transcriptional activity occurs in bursts, modulating the instantaneous fraction of transcriptionally active nuclei in **b**.

Tissue-wide transcriptional dynamics arise from the switch-like regulation of the instantaneous fraction of transcribing cells. How do tissue-level patterns of mRNA arise from the transcriptional activities of individual cells? Such tissue-level control could be implemented in two possible ways[44,45]. One strategy consists of modulating the single-cell rate of transcription across all cells in a graded, analogue fashion (Fig. 4a, top). Alternatively, transcriptional control could work like a switch, where the fraction of cells transcribing above basal uninduced levels is modulated across the tissue (Fig. 4a, bottom). Several *Drosophila* enhancers invoke both strategies simultaneously[9,17]. Single time-point measurements in plants[46,47] and live-imaging studies in cell culture[39] have also provided evidence for switch-like control.

We found that, as transcriptional induction ensues, the instantaneous fraction of cells that are actively transcribing increases (Fig. 3b). In addition, the level of transcription in active cells can also fluctuate (Fig. 3c). We therefore sought to determine the extent to which each regulatory strategy gives rise to tissue-wide control of the mean mRNA production rate. To this end, we expressed the total bulk transcriptional activity in terms of the quantitative contribution of each regulatory strategy as

$$\frac{\sum_i \mathrm{fluo.}_i(t)}{N_{\mathrm{total}}} = \frac{\sum_i \mathrm{fluo.}_i(t)}{N_{\mathrm{active}}(t)} \times \frac{N_{\mathrm{active}}(t)}{N_{\mathrm{total}}} \quad (1)$$

Here, $\mathrm{fluo.}_i(t)$ is the fluorescence of the ith cell at time point t, $N_{\mathrm{active}}(t)$ is the instantaneous number of active cells, and N_{total} is the total number of cells. Thus, the term on the left-hand side of equation (1) corresponds to the mean tissue-wide transcription rate, the first right-hand side term corresponds to the mean transcription

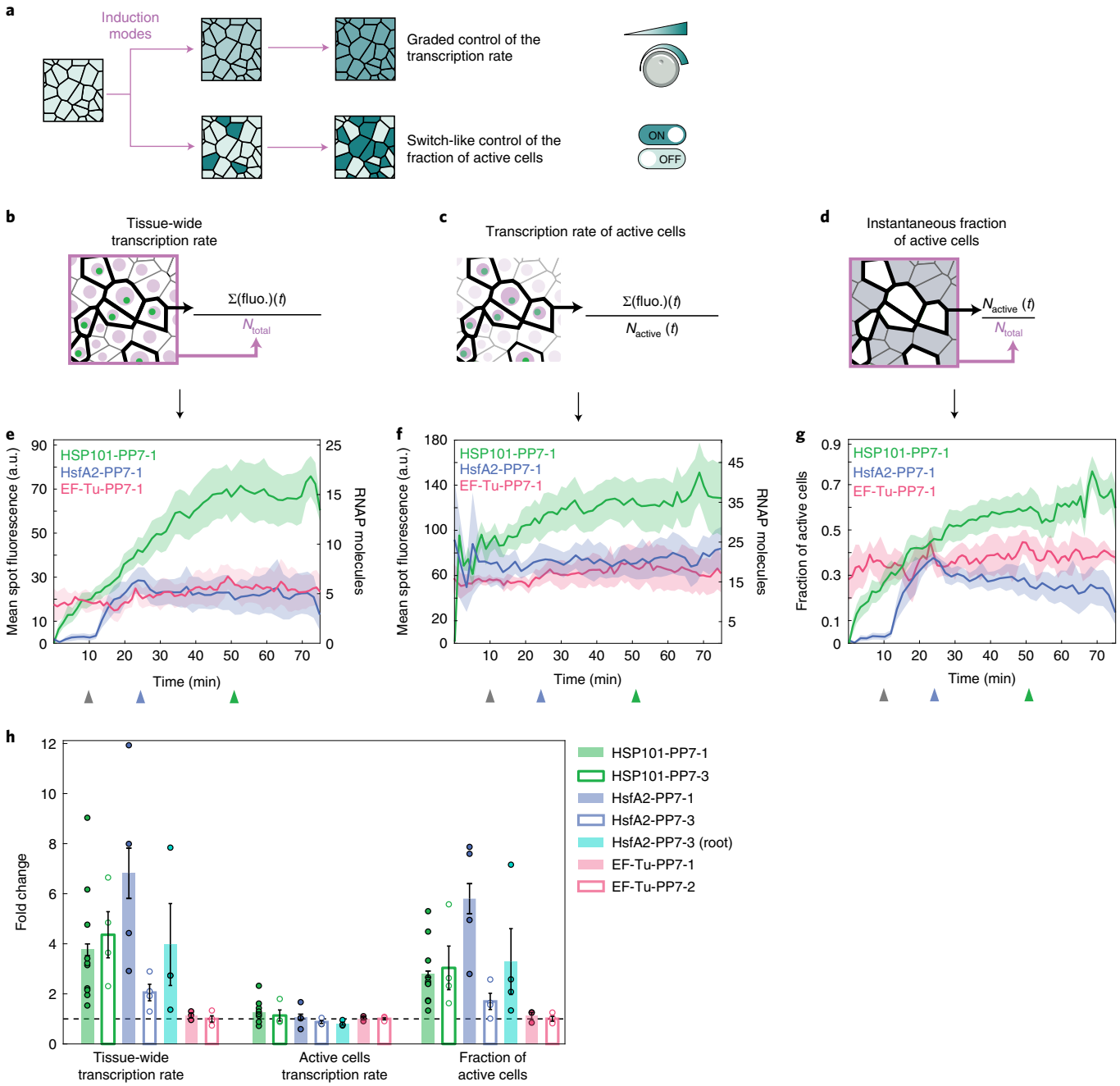

Fig. 4 | Single-cell regulatory strategies determining tissue-wide transcriptional dynamics. a, Tissue-wide transcriptional control can be achieved through two non-exclusive regulatory modes: the graded modulation of the rate of transcription across cells (indicated by a volume control knob), or the switch-like regulation of the fraction of actively transcribing cells (indicated by a switch). **b**, The tissue-wide transcription rate is obtained by—at each time point—adding up the fluorescence (fluo.) of all spots and dividing by the total number of nuclei N_{total}, regardless of their transcriptional state. **c**, The transcription rate of active cells is calculated by—in each frame—adding the fluorescence of all spots and dividing by the number of nuclei with spots in that frame $N_{active}(t)$. **d**, The fraction of active cells corresponds to the number of nuclei that have detectable reporter transcription at a given time $N_{active}(t)$ divided by the total number of nuclei N_{total}. **e**–**g**, Data from *Arabidopsis* lines carrying inducible promoters HSP101-PP7-1 (green) and HsfA2-PP7-1 (blue), and a line with the constitutive reporter EF-Tu-PP7-1 (red). Time $t = 0$ corresponds to the frame at which spots were first detected. **e**, Mean tissue transcription rate. **f**, Mean transcription rate across active cells. **g**, Mean instantaneous fraction of actively transcribing cells. **h**, Fold change in the mean tissue-wide transcription rate compared with the fold change in the mean transcription rate of active cells and in the fraction of active cells, defined as the ratio between the value at its peak and at $t = 10$ min for HSP101-PP7-1 (grey versus green arrowheads in **e**–**g**) and HsfA2-PP7 (grey versus blue arrowheads in **e**–**g**). For EF-Tu-PP7, the fold change was calculated between 10 and 30 min. The empty and light blue bars correspond to data obtained from independent transgenic lines shown in Supplementary Fig. 20. The horizontal dashed line indicates a fold change of 1. Shaded regions in **e**–**g** show the s.e.m. calculated across $n = 8$ (HSP101-1), 5 (HsfA2-1) and 3 (EF-Tu-PP7-1) biological replicates. Data in **h** are mean ± s.e.m. of $n = 8$ (HSP101-1), 4 (HSP101-3), 5 (HsfA2-1), 3 (HsfA2-3), 3 (HsfA2-3 (root)), 3 (EF-Tu-1) and 3 (EF-Tu-2) biological replicates.

rate across active cells, and the second right-hand side term corresponds to the instantaneous fraction of active cells.

To determine how the resulting tissue-level transcriptional dynamics arises from the two contributions on the right side of equation (1), we first determined the tissue-wide transcription rate at each time point (corresponding to the left side of the equation), by adding the fluorescence of all spots in each frame and then dividing by the total number of nuclei in the field of view (Fig. 4b). This calculated tissue-wide transcription rate is akin to the data typically obtained using a time series of bulk sampling experiments. The tissue-wide transcription rate of HSP101-PP7-1 and HsfA2-PP7-1 increased upon induction, while that of the constitutive EF-Tu-PP7-1 reporter line remained constant throughout the experiment (Fig. 4e).

To determine whether the graded modulation of the transcription rate among active cells contributes to the mean tissue transcription rate, we calculated the mean spot fluorescence across actively transcribing cells only (the first term on the right side of equation (1) (Fig. 4c)). Further, to determine the contribution of the switch-like type of regulation, we computed the instantaneous fraction of cells in which we detect reporter activity (the second term on the right side of equation (1) (Fig. 4d)). Our calculations revealed that the temporal modulation of the transcription rate among active cells remained relatively constant throughout induction (Fig. 4f). By contrast, the fraction of active nuclei was strongly modulated as a result of induction (Fig. 4g). The dynamics of the fraction of active cells were qualitatively comparable to the mean tissue transcription rate (compare Fig. 4e,g).

To quantify the relative contribution of each of these regulatory strategies to the overall transcriptional dynamics, we measured the fold change of each term in equation (1). We defined this fold change as the ratio between the value of each magnitude at peak induction (blue and green arrowheads in Fig. 4e–g) and at 10 min, shortly after the beginning of the response (grey arrowhead in Fig. 4e–g). For both heat-inducible promoters, the fold change in the mean transcription rate across active cells was close to one, indicating no substantial change over time (Fig. 4h). In contrast, the fold change in the instantaneous fraction of active cells was almost identical to that of the total activity (Fig. 4h).

To determine the generality of our results, we performed these experiments and analysis on a second set of independent transgenic lines of all three promoters. Our analyses yielded similar results (Supplementary Fig. 20). In addition, we tested whether these findings also apply to other tissues. Measurements of HsfA2-PP7 expression in root tips showed that, indeed, the rate of transcription of responsive cells is stable, whereas the number of active nuclei is modulated over time (Fig. 4g,h and Supplementary Fig. 20).

Thus, the duration of the treatment does not impact the rate of transcription of individual actively transcribing cells: when an individual cell transcribes, it tends to do so, on average, at a characteristic, relatively stable level regardless of induction time (Supplementary Fig. 21). Instead, the time under stress modulates the tissue-wide transcription rate by increasing the probability that each individual cell switches from basal undetectable transcription to a high-activity state.

Allele-specific regulation underlies most tissue-wide heterogeneity in mRNA production in living plants. Although physiological responses occur at the tissue level, each cell must bear the phenotypic consequences of its individual gene-regulatory behaviour in response to stress. Studies of microorganisms and mammalian cells in culture have revealed that single-cell transcriptional responses to outside stimuli are often highly variable, leading researchers to posit that organisms possess mechanisms to buffer this 'noise' or to leverage variability to drive the adoption of cellular fates that, for example, provide resistance against environmental insults such as antibiotics[48]. However, little is known about the level, functional roles and underlying molecular mechanisms of transcriptional noise in shaping stress responses in multicellular systems like plants[49,50].

Although, on average, the rate of transcription of our heat-responsive reporters in active cells did not substantially change with the duration of the heat treatment (Fig. 4c), at any given time point, the levels of activity across cells spanned more than two orders of magnitude (Fig. 5a). This behaviour of actively transcribing cells, combined with asynchronous activation (Fig. 3c) and the presence of cells that are transiently or permanently transcriptionally inactive (Fig. 4g and Supplementary Fig. 13) give rise to a wide distribution in the inferred amount of mRNA produced per cell (Fig. 5b). This distribution spans more than three orders of magnitude, with a coefficient of variation (s.d. divided by the mean) of approximately 1.6. While this variability might seem exceedingly high, it is on the same order as in other eukaryotic systems[51–53]. Simulating a constant, homogeneous mRNA degradation rate does not considerably alter the spread of these distributions (Supplementary Fig. 22).

What are the molecular sources of this cell-to-cell variability in the amount of mRNA produced (Fig. 5c)? One hypothesis invokes differences in composition across cells. For example, differences in cell cycle stage[54], concentration of general transcriptional machinery[55] or concentration of specific transcription factors[50] can generate cellular heterogeneity (Fig. 5c, left). Alternatively, because at the local gene-level transcription depends on a relatively small number of molecules, it is subjected to the stochasticity inherent to biochemical reactions. This can lead to variability even among otherwise identical cells (Fig. 5c, right).

To distinguish between these two types of sources of noise, it is necessary to compare the expression of alleles belonging to the same cell with that of alleles in nearby cells[54,56]. Intuitively, factors extrinsic to the gene that operate at the cellular level will lead to alleles in a cell behaving similarly to each other but differently to those in other cells. By contrast, processes intrinsic to the gene operating at the local level will lead to alleles in the same cell behaving differently even if they are exposed to the same extrinsic factors. By decomposing the total variability into variability across allele pairs within each cell and variability across cells, extrinsic and intrinsic sources can be quantified without a priori knowledge of their molecular identity[56] (Supplementary Section 1.4).

A previous measurement of gene-expression noise in *Arabidopsis* using constitutively expressed fluorescent proteins found that extrinsic factors explain most of their cellular heterogeneity[57]. However, it is unclear how noise in accumulated protein relates to transcriptional variability that we can now measure using PP7, and whether there are differences between constitutive and regulated promoters.

To determine the contribution of each type of transcriptional noise, we imaged T2 *Arabidopsis* individuals homozygous for the reporter, which display up to two fluorescent spots per nucleus in diploid cells (Fig. 5d, top and Supplementary Video 6). Four traces originating from two nuclei indicate that the transcriptional activity of alleles in the same nucleus can be more similar to each other than the activity of alleles in different nuclei (Fig. 5d, bottom), suggesting an important role for extrinsic noise in transcriptional variability. However, our measurements also revealed that allele pairs in the same nucleus are not necessarily in the same transcriptional state: nuclei are approximately equally divided between populations in which two, only one, or no alleles exhibit a transcription spot (Fig. 5e). This suggests that the decision of alleles to become active is intrinsic to each allele. Thus, qualitatively, we have identified that both intrinsic and extrinsic contributions can potentially underlie the total transcriptional noise.

To determine the quantitative contribution of each source of variability to the single-cell distribution of mRNA produced, we compared the mRNA produced by alleles in the same nucleus to

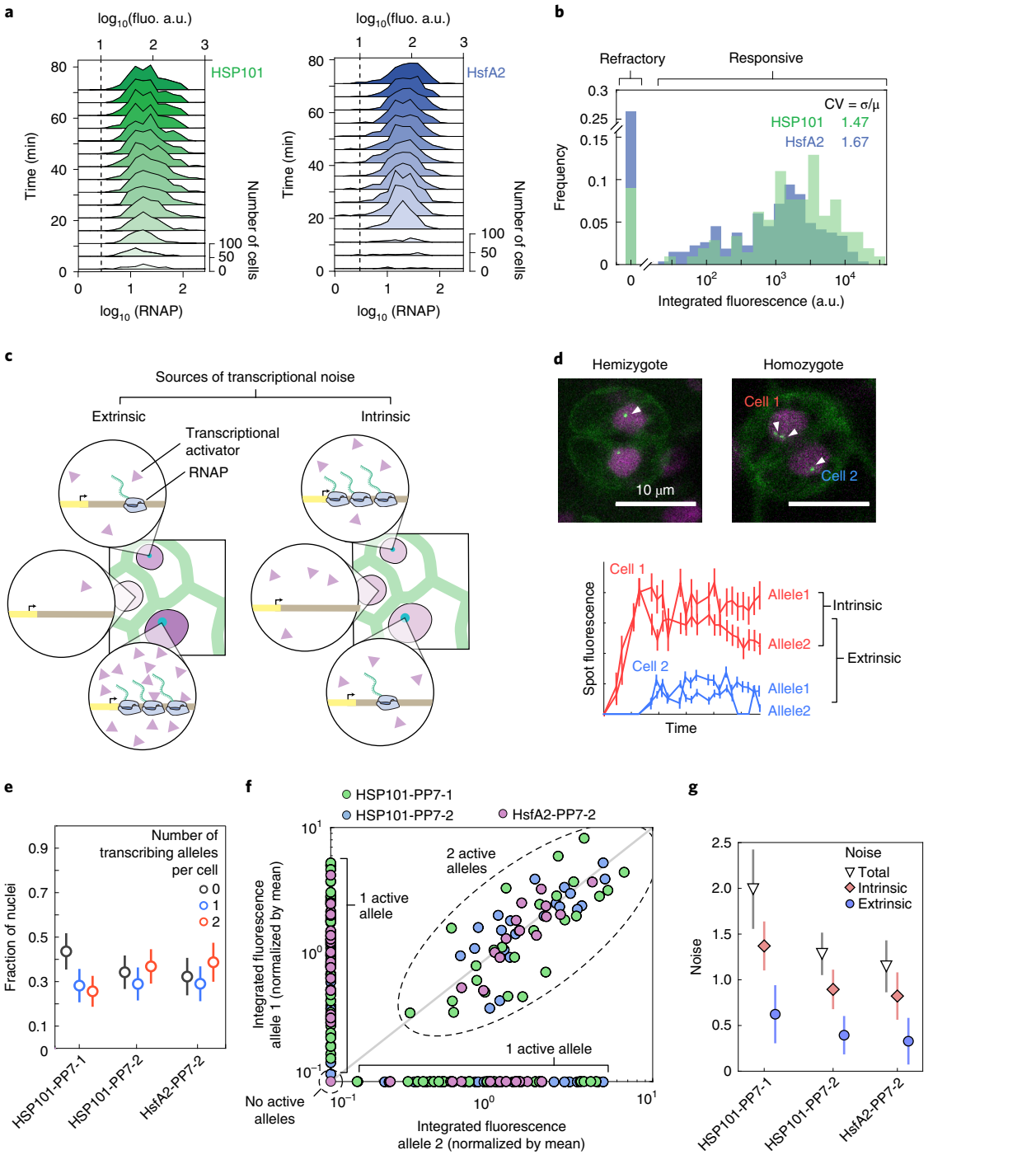

Fig. 5 | Allele-specific processes explain most of the cellular heterogeneity in produced mRNA in *Arabidopsis*. **a**, Histograms of spot fluorescence over time for the combined replicates of Fig. 4. The dashed line indicates the detection threshold determined in Fig. 2d. **b**, Histograms of predicted total produced mRNA per cell across all replicates from Fig. 4. Shown is the CV (standard deviation/mean) of each distribution. **c**, Schematic of extrinsic (left) and intrinsic (right) sources of transcriptional noise. Extrinsic noise arises from cellular differences in the concentration of regulatory molecules (purple triangles), such as transcription factors, whose abundance is common to all alleles, whereas intrinsic noise captures differences among cells with identical composition due to local processes at each allele such as the inherent stochasticity of biochemical reactions. **d**, Two-allele experiment to decompose the total transcriptional variability into intrinsic and extrinsic noise. Top: guard cells—which are obligate diploids[35]—expressing HSP101-PP7. White arrowheads indicate transcription spots corresponding to one or two alleles of the reporter transgene in homologous chromosomes. In the homozygote, it is possible for only one allele to be active in different cells. Bottom: spot fluorescence traces from homozygous cells shown on top, the error bars correspond to the uncertainty in fluorescence quantification as described in Methods. **e**, Fraction of nuclei with zero, one or two spots in heat shock-treated homozygous plants at the frame with the maximum number of visible spots. **f**, Scatter plot of the integrated spot fluorescence normalized by the mean for pairs of alleles belonging to the same nucleus. Undetected spots were assigned a value of zero and plotted on the *x*- and *y*-axes. **g**, Decomposition of the total variability in **f** into extrinsic and intrinsic components shows comparable contributions of both components to the total noise, with the intrinsic component explaining most of the variability. Error bars in **e** and **g** are bootstrapped errors (1,000 samples) taken over 128, 111 and 69 nuclei obtained from two biological replicates of HSP101-PP7-1, HSP101-PP7-2 and HsfA2-PP7-2, respectively.

the mRNA produced by alleles in different nuclei, following the method used in ref. [56] (details about this calculation are presented in Supplementary Section 1.4 and Supplementary Fig. 23). Transgenes in *Arabidopsis* are frequently inserted as tandem repeats[58], which cannot be optically resolved from each other. We used qPCR to determine the number of tandem insertions in HSP101-PP7-1 and HsfA2-PP7-1 and found that these lines are likely to contain 2 and 3 transgenes per locus, respectively. To show that the results from this noise analysis do not qualitatively depend on the number of transgene copies per insertion, we identified additional single-insertion *Arabidopsis* lines (HSP101-PP7-2 and HsfA2-PP7-2) for which we confirmed the presence of a single transgene copy per insertion locus using qPCR (Supplementary Fig. 10 and associated calculations in Supplementary Section 1.3). Figure 5f presents the integrated spot fluorescence of allele pairs belonging to the same nucleus in homozygous plants of HSP101-PP7-1 and two additional lines with a single transgene copy per insertion. Our calculation of the noise components revealed that intrinsic sources explain most (about two-thirds) of the variability in all of the lines tested (Fig. 5g).

We next sought to further investigate possible sources contributing to the extrinsic noise. Studies in plants[42,50] have shown that cell size is positively correlated with gene expression, making it a potential source of extrinsic noise. We found that nucleus volume (a good proxy for cell size[36]) explains only 10–30% of the cell-to-cell variability in expression (Supplementary Fig. 24). The lack of a strong correlation between transcription and nucleus size might be due to all nuclei in our sample being relatively similar in size (Supplementary Fig. 11). An additional source of extrinsic noise could be cell-type identity. For example, the expression dynamics of guard cells and non-guard cells, both present in our field of view, could contribute to this noise. As shown in Supplementary Fig. 25, we did not find a consistent, statistically significantly difference in produced mRNA between guard cells and the rest of the cells. Thus, the molecular identity of the sources of extrinsic noise remain to be identified.

In sum, despite the presence of extrinsic noise, our results demonstrate that most of the cellular heterogeneity in the transcriptional response to heat shock is not due to cells having a different chemical composition. Instead, stochastic processes at the level of each individual allele explain most of the cell-to-cell differences in the amount of mRNA produced per cell. Importantly, while here we have focused on the noise in the amount of produced mRNA, further insights can be drawn from examining the sources of molecular variability in, for example, instantaneous transcriptional activity (Supplementary Fig. 26).

Discussion

Over the past few decades, it has become clear that the averaging resulting from bulk tissue sampling obscures important details about the spatial control of cellular processes in both plants and animals. In plants, this limitation has motivated recent advances in single-cell RNA sequencing[59]. However, these measurements depend on the previous history of RNA transcription and degradation and thus obscure information about regulatory dynamics. Further, single-cell sequencing technologies tend to sacrifice spatial information. While enabling technologies to light up the process of transcription and its control in real time, in single cells and whole animals, have been developed, plants have remained surprisingly neglected.

Here, by implementing the PP7 and MS2 systems to fluorescently label nascent RNA molecules in plants, we have shown that it is possible to count the number of RNAP molecules actively transcribing individual alleles in single living cells of tobacco and *Arabidopsis* as they respond to their environment. This technical advance yielded unprecedented access to the temporal history of activity of individual alleles, making it possible to uncover distinct modes by which single-cell transcriptional activity in plants leads to tissue-wide gene-expression dynamics.

Using this technique, and consistent with similar observations in other systems[9,17,39], we discovered a fraction of transcriptionally refractory cells that do not transcribe above our detection limit of approximately three active RNAP molecules per gene, regardless of induction conditions (Fig. 4d). Single-molecule RNA fluorescence in situ hybridization experiments in *Arabidopsis* roots found that at any given time approximately 20% of cells are transcriptionally inactive for the constitutively expressed *PP2C* gene[60]. However, unlike the live-imaging approach developed here, single-molecule RNA fluorescence in situ hybridization relies on fixed samples; it cannot determine whether this inactive state was transient or stable. Arguably, what we refer to as inactive nuclei might be transcribing at a low, basal rate and not be completely transcriptionally silent. However, in cells such as plant cells, that divide slowly, extremely infrequent transcription is sufficient to sustain low mRNA levels, particularly if these mRNA molecules have long half lives. Thus, it is not rare for genes that are expressed at low levels to be free of polymerases for tens of hours in any given cell, even though their mRNA is detected at the population level[61].

We also found that tissue-wide transcriptional induction dynamics are the result of the temporal modulation in the fraction of cells that switch to a transcriptionally active state, and not of the graded control of the transcription rate of active cells (Fig. 4c). This form of regulation has been hypothesized to be at play in the regulation of the *FLC* gene in response to temperature[47] and in the commitment to xylem cell fate in response to the VND7 transcription factor[46]. Using our technologies, it should now be possible to directly test these models.

These single-cell behaviours may seem difficult to reconcile with previous bulk time-course experiments showing that the mRNA molecules of inducible genes are present under control conditions and accumulate gradually in response to stress treatments[26,62]. Yet, ample evidence from single-cell studies has shown that single-cell observations rarely match the average cell behaviour captured by bulk experiments[48,63].

Gene expression can vary greatly from cell to cell in microbial and animal species[48]. By making it possible to measure cell-to-cell transcriptional variability in real time in living plant cells, we confirmed that plants are no exception to this widespread presence of transcriptional variability. The single-locus resolution of our method allowed us to determine that cell-to-cell variability in mRNA production arises mainly from stochastic processes instrinsic to each allele (Fig. 5g). Studies in in vitro cell cultures have found that gene-expression noise can have profound consequences for cellular survival[48]; however, the role of transcriptional noise in plant stress responses remains an open question[49]. We envision that the strategy applied here to systematically dissect transcriptional heterogeneity in *Arabidopsis* and tobacco will shed light on this interplay between transcriptional variability and stress response. Further, it will be interesting to examine how some unusual aspects of plant cell biology and genetics can buffer transcriptional noise. For example, cytoplasmic connections through plasmodesmata could play a role in short-range sharing of gene products, averaging out extrinsic noise as observed in syncytial systems[64]; multiple genome copies per nucleus in mature plant cells may provide further opportunities to average out intrinsic noise across alleles. Similarly, we speculate that the conspicuous retention of large numbers of seemingly redundant gene paralogues in plants may also help buffer intrinsic fluctuations in individual genes[65].

Our approach requires access to a confocal microscope and to transgenesis tools, and should therefore be relatively easy to apply to many biological problems in plant development and physiology. However, imaging deep into live tissues with the resolution necessary to resolve diffraction-limited spots remains a challenge, particularly in plants. Advances such as multiphoton imaging, lattice light-sheet microscopy and adaptive optics will overcome this limitation[66].

Lacking single-polymerase resolution currently limits the applicability of MS2 and PP7 to genes transcribed at relatively high rates.

A transcription initiation rate of 1.5 RNAP min^{-1}, corresponding to our detection limit of 3 elongating RNAP molecules on an average *Arabidopsis* gene, could be sufficient to sustain slow transcriptional processes operating at long developmental timescales. For example, the *FLC* gene, a key seasonal developmental regulator in *Arabidopsis* is rarely occupied by more than one elongating RNAP at a time[42] which may explain why previous attempts at visualizing nascent *FLC* mRNAs in live *Arabidopsis* plants have failed[67]. Increasing the number of stem–loop repeats could be a viable strategy to enable the measurement of weakly expressed genes[68]. A growing interest in live imaging of transcription combined with advances in fluorophore chemistry[69] as well as in the PP7 and MS2 technologies themselves[70] offer hope for breaking this detection threshold.

It will undoubtedly be of interest to correlate the activities of genes by visualizing their transcription simultaneously. This multiplexing is already possible for two genes using MS2 and PP7. A third colour could be added by implementing interlaced MS2 and PP7 loops[22]. To further extend the palette, it should be possible to engineer other orthogonal RNA-binding proteins–RNA aptamer pairs[71].

Finally, and more generally, the random integration of transgenes in plants and their associated genomic rearrangements[58] makes it challenging to dissect the roles of regulatory sequences at their endogenous genomic locations. In addition, if the goal is to study the behaviour of endogenous genes, reporter constructs might not be sufficient since they may not faithfully recapitulate all aspects of endogenous regulation. Delivery of DNA to specific genomic locations using clustered regularly interspaced short palindromic repeats (CRISPR)–CRISPR-associated protein 9 (Cas9) or sequence-specific recombinases promise to address these problems and unleash the potential of quantitative reporters of gene expression.

In this study, we focused on a simple step in the plant's use of temperature as a signalling input. More complex treatments have been previously used to show that plants can mount specific responses to inputs, such as memory in response to pulses of heat shock[38] and nonlinear integration of combinations of high light and temperature stress[4]. By administering experimental treatments while simultaneously measuring their effects on gene regulation, it will be possible to determine how these operations are performed at the cellular level. In addition, the sub-nuclear resolution of nascent RNA tagging could make it possible to resolve long-standing issues in plant signalling, such as the role of protein aggregates or 'nuclear speckles' that are pervasive in light-responsive signalling pathways in plants[72].

In conclusion, by enabling the measurement of transcription at high spatiotemporal resolution, the PP7 and MS2 methods introduced here close a critical technological gap in plant biology. These new technologies open new avenues of inquiry and will make it possible to quantitatively interrogate transcriptional control in living plants and to engage in the discourse between theory and experiment that has characterized the study of gene regulation in single cells and animal tissues over the past two decades[73].

Methods

Plasmids and *Agrobacterium* strains. All plasmid sequences used in this study can be accessed from a public Benchling folder (https://benchling.com/garcialab/f_/cYU9YGaf-imaging_transcription_plants/). All plasmids used in this study are available from Addgene (https://www.addgene.org/browse/article/28215330/). All vectors were based on pCambia derivatives and transformed into the GV3101::pMP90 Agrobacterium strain by electroporation. Plasmids confering kanamycin resistance in plants (that is, reporter constructs) were based on pCambia2300. Plasmids confering Hygromycin resistance in plants (that is, PCP, MCP and nanocages constructs) were based on pCambia1300. A list of all the plasmids used in this study along with their link to Benchling and Addgene can be found in Supplementary Table 1. The *Arabidopsis* gene identifiers associated with genomic sequences used in these plasmids are listed in Supplementary Table 2.

Plant growth conditions. *N. benthamiana* (tobacco) plants were grown in a greenhouse under natural light conditions prior to agroinfiltration. Following infiltration, tobacco plants were kept under 30 µE of constant light. *Arabidopsis* plants used for experiments were grown in 0.5× MS agar containing 50 µg $µl^{-1}$ kanamycin under short day conditions (8 h of 30 µE light per day) for 4–6 weeks before imaging.

Agroinfiltration. Agrobacterium glycerol stocks were streaked on LB plates containing 50 µg $µl^{-1}$ kanamycin and 50 µg $µl^{-1}$ gentamycin. Fresh colonies were grown overnight in liquid LB containing the same antibiotic concentrations, spun down and resuspended in an equal volume of infiltration buffer (10 mM MES pH5.6, 10 mM $MgCl_2$, 150 µM acetosyringone). Cells were incubated for 2–4 h in infiltration buffer shaking at room temperature after which the cultures were diluted 1:3 to an optical density at 600 nm (OD_{600}) of approximately 0.3. In experiments that required combining strains, coat protein and reporter strains were mixed in a 3:1 ratio (the exact ratio does not qualitatively affect the results). In PP7 and MS2 experiments, infiltrated leaves were imaged approximately 2 d after infiltration. For absolute calibration experiments, plants were imaged 12–18 h after infiltration.

Generation of transgenic *Arabidopsis* lines. To generate lines carrying both PCP–GFP and PP7 reporters, we followed a sequential transformation approach. We first selected PCP–GFP lines in 35 µg ml^{-1} hygromycin and kept lines exhibiting moderate levels of fluorescence and no obvious growth phenotype. Next, we transformed T1 or T2 PCP–GFP individuals with PP7 reporter *Agrobacterium* strains and selected transformants in 50 µg ml^{-1} kanamycin and 35 µg ml^{-1} hygromycin. Individuals T1 for the PP7 construct were screened for nuclear mScarlet fluorescence and presence of transcription spots matching previous knowledge about the activity of the corresponding endogenous gene. A list of the lines used in this study can be found in Supplementary Table 3.

Determining the number of unlinked reporter transgene insertions. To select lines carrying a single-insertion reporter locus we plated approximately 60 T2 seeds in MS plates containing kanamycin and counted the ratio of survivors. This ratio was divided by the survival ratio in plates containing no antibiotics. A χ^2-test was used to determine whether the product of these two ratios was statistically different from the expected ratio of 0.75. To confirm the absence of two or more unlinked reporter loci we examined transcription spots in guard cells. Unlike other leaf cell types, these cells are exclusively diploid[35] and therefore the presence of a single spot per guard cell nucleus in a T1 individual confirms the absence of unlinked insertions.

Heat shock treatments. To control the sample temperature in the microscope stage we used an OkoLabs H101-LG temperature chamber calibrated to achieve a maximum of approximately 39 °C. The temperature experienced by the sample was calibrated using an electronic probe. The walls of the chamber were kept at 54 °C for the sample to reach a steady-state temperature of 39 °C. To estimate the difference in temperature between the centre of the field of view and its edges, we simplify the problem by approximating it to a radial temperature gradient going outwards from the centre of the sample, with the centre being at the sample temperature (39 °C) and the edge at the temperature of the walls of the chamber (54 °C), located 5 cm away from the centre. We can then use a linear approximation for the temperature gradient, which results in a gradient of 0.0003 °C $µm^{-1}$. This means that the difference of temperature from the centre of the field of view to its edge is 0.0003 °C $µm^{-1}$ × 45 µm ≈ 0.015 °C. The heat shock treatment used for the RT–qPCR experiment in Fig. 2a was performed as follows: whole 4- to 6-week-old plants were placed in 1.7 ml plastic tubes containing 200 µl water. The sample corresponding to time = 0 min was immediately taken out of the tube, quickly tapped dry, transferred to a new tube containing silica beads and frozen in liquid nitrogen. The rest of the samples were transferred to a 39 °C heat block and removed at set times. Plants were then quickly tapped dry and frozen in liquid nitrogen.

Microscopy setup and image acquisition. In tobacco experiments, a piece of infiltrated leaf spot was mounted in water between a glass slide and a glass coverslip with the abaxial (bottom) side facing the objective. In *Arabidopsis* experiments, full 2-to 4-day-old leaves from 4- to 6-week-old plants were detached and mounted in tap water between a gas permeable cellophane membrane (Lumox film; Starstedt) and a glass coverslip with the adaxial (top) side facing the objective. All samples were imaged close to the base of the leaf blade immediately after mounting. All data was taken in a Leica SP8 confocal microscope with a white light laser using a ×63 oil objective. The dimensions of the field of view were 92.26 × 46.09 µm using 1,052 × 512 pixels, resulting in a pixel size of 90 nm. *z*-Stacks consisting of 25 slices of 0.5 µm each were taken every 60 s, accumulating fluorescence 3 times over lines. The beginning of each stack was set to the uppermost nucleus in the leaf epidermis. For GFP, excitation was 488 nm and emission was 498–559 nm. For mScarlet, excitation was 569 nm, emission was 579–630 nm. For chlorophyll, excitation was 488 nm, emission was 665–675 nm. To ensure quantitative consistency across experiments, the 488 nm laser power was calibrated to 10.5 µW (approximately 5% laser power) at the beginning of each imaging session using a power meter. The percentage intensity of the 569 nm laser line was kept consistent across experiments at 5%. To minimize the background signal from endogenous plant fluorophores, we used the gating function of the HyD detectors to limit detection to a time window between 0.3 and 6 ns after excitation.

RT–qPCR. Total RNA was extracted using the Qiagen RNeasy kit following the manufacturer's instructions. Reverse transcription was performed using the Qiagen Omniscript kit with a primer mix of random 10mers (10 µM final concentration) and 15mer oligo dT primers (1 µM final concentration). A negative control was performed adding water instead of reverse transcriptase. mRNA abundance was calculated by the ΔC_T method. Primers for endogenous *HSP101* were 5′-GGTCGATGGATGCAGCTAAT-3′ and 5′-CTTCAAGCGTTGTAGCACCA-3′ (ref. [74]). Primers for the *Actin2* standard were 5′-CGCTCTTTCTTTCCAAGCTCAT-3′ and 5′-GCAAATCCAGCCTTCACCAT-3′ (ref. [75]). Primers for the reporter mRNA were 5′-GGGTTCATCAGAGTGCCAGAG-3′ and 5′-AGGCAGAGCGACACCTTTAG-3′. A negative control experiment was performed under identical conditions replacing the reverse transcriptase enzyme with water.

Image analysis. *Spot fluorescence and tracking.* Raw image stacks of the coat protein channel were used to identify fluorescent punctae corresponding to transcription spots using the ImageJ implementation of the 3D Trainable Weka Segmentation toolbox[76]. Following ref. [17], after segmentation, spots in each *z*-slice were fitted to a 2D Gaussian. The *z*-slice with the largest Gaussian amplitude was selected for the spot fluorescence calculation. Spot fluorescence corresponds to the sum of pixel intensity values in a circle with a radius of 1.08 µm centred around the centre of the fitted Gaussian minus the background fluorescence offset.

The fluorescence error per spot shown in Figs. 1e and 5d was obtained on the basis of the approach from ref. [9]. First, in each frame we calculated the fluorescence offset from the fitted baseline obtained from the Gaussian fitting procedure described above. This results in a time trace of offset values for each spot time trace (example in Supplementary Fig. 6g). Next, we fitted a spline to this time trace and calculated the root-mean-square deviation of offset values with respect to the spline. This value represents the fluctuations of the background intensity per pixel. Finally, we multiplied this deviation by the same integration area used for transcription spots to obtain an error in the same magnitude. False-negative and false-positive spots were corrected manually.

Nuclear segmentation and spot tracking. Maximum-intensity projections of the nuclear marker channel were used for nuclear segmentation using the ImageJ implementation of the 2D Trainable Weka Segmentation toolbox[76] or a custom-written Matlab pipeline. False-negative and false-positive nuclei were then manually corrected. Spots were assigned to nuclei on the basis of physical overlap. Tracking of spots over time was based on nuclear tracking and manually corrected whenever errors were found.

Nucleus fluorescence. A binary mask of segmented nuclei was applied to the PCP–GFP or Histone 2B–mScarlet channel. For each *z*-slice in each frame, the mean fluorescence across pixels within each nucleus area was calculated. As a result, in each frame, the fluorescence intensity of a given nucleus has the form of a 'column' of intensities over *z*. Next, in each frame we took the brightest *z*-slice in this column as the fluorescence value corresponding to the concentration of bright fluorescent protein in a given nucleus at a given time point.

Determining transgene copy number by qPCR. Genomic DNA was extracted from leaf tissue using cetyl trimethylammonium bromide and phenol:chlorophorm precipitation. Primers used to amplify the reporter transgene were 5′-gacgcaagaaaaatcagagagatcc-3′ and 5′-ggtttctacaggacggaccatacac-3′. Primers used to amplify a region near the *Lhcb3* gene used as an internal genomic control were 5′-acaggtttggtcaagtcaattacga-3′ and 5′-atggtttccatgaatactgaacacg-3′. The final concentration of genomic DNA per reaction was 0.75 ng. For a more detailed explanation of the calculations and controls related to this experiment see Supplementary Section 1.3.

Absolute calibration using nanocages. Tobacco leaves were infiltrated with agrobacterium strains containing plasmids where the promoter of the *Arabidopsis UBC1* gene (1,138 bp upstream of the AT1G14400 start codon) was used to drive the 60mer monomer fused to either one or two mGFP5-coding sequences. The same scheme was used to express the monomers of the 60meric GEM. The amino terminus of the rabbit cytochrome P450 CII1 was added as an N-terminal tag to target the protein fusions to the cytosolic side of the endoplasmic reticulum to slow down their diffusion. Samples were imaged no later than 16 h after infiltration since long incubation periods resulted in the appearance of large GFP aggregates. To image the GFP nanocages in mesophyll cells, the abaxial epidermis was first removed. This is necessary to obtain a large number of structures in the field of view. The fluorescence of nanocages was calculated with the same analysis pipeline used for transcription spots. The imaging conditions were identical to the ones used in transcription experiments except that a 5 times stronger laser power was used for the 488 nm line to increase the signal. After obtaining the fluorescence of individual nanocages their fluorescence was divided by five before calculating their mean fluorescence. The validity of this operation is due to the linearity of fluorescence intensity and laser power under our conditions for both nanocages and PP7 spots (Supplementary Fig. 8).

Reporting Summary. Further information on research design is available in the Nature Research Reporting Summary linked to this article.

Data availability

Raw and analysed data are available upon request. All plasmids used in this study are listed in Supplementary Table 1 and were submitted to the AddGene public repository. *Arabidopsis* seeds are listed in Supplementary Table 3 and are available from the Arabidopsis Biological Resource Center stock centre and/or upon request from the Niyogi laboratory. Source data are provided with this paper.

Code availability

All code used to analyse raw data can be found in the public GitHub repositories https://github.com/GarciaLab/mRNADynamics and https://github.com/GarciaLab/PlantPP7.

Received: 15 October 2020; Accepted: 22 June 2021;
Published online: 9 August 2021

References

1. Suzuki, N. et al. Ultra-fast alterations in mRNA levels uncover multiple players in light stress acclimation in plants. *Plant J.* **84**, 760–772 (2015).
2. Leivar, P. et al. Definition of early transcriptional circuitry involved in light-induced reversal of PIF-imposed repression of photomorphogenesis in young *Arabidopsis* seedlings. *Plant Cell* **21**, 3535–53 (2009).
3. Krouk, G., Mirowski, P., LeCun, Y., Shasha, D. E. & Coruzzi, G. M. Predictive network modeling of the high-resolution dynamic plant transcriptome in response to nitrate. *Genome Biol.* **11**, R123 (2010).
4. Zandalinas, S. I., Fritschi, F. B., Mittler, R. & Lawson, T. Signal transduction networks during stress combination. *J. Exp. Bot.* **71**, 1734–1741 (2020).
5. Gould, P. D. et al. Coordination of robust single cell rhythms in the *Arabidopsis* circadian clock via spatial waves of gene expression. *eLife* **7**, e31700 (2018).
6. Kollist, H. et al. Rapid responses to abiotic stress: priming the landscape for the signal transduction network. *Trends Plant Sci.* **24**, 25–37 (2019).
7. Balleza, E., Kim, J. M. & Cluzel, P. Systematic characterization of maturation time of fluorescent proteins in living cells. *Nat. Methods* **15**, 47–51 (2018).
8. Lucas, T. et al. Live imaging of bicoid-dependent transcription in *Drosophila* embryos. *Curr. Biol.* **23**, 2135–2139 (2013).
9. Garcia, H. G., Tikhonov, M., Lin, A. & Gregor, T. Quantitative imaging of transcription in living *Drosophila* embryos links polymerase activity to patterning. *Curr. Biol.* **23**, 2140–2145 (2013).
10. Lee, C. H., Shin, H. & Kimble, J. Dynamics of notch-dependent transcriptional bursting in its native context. *Dev. Cell* **50**, 426–435 (2019).
11. Park, S. J. et al. Optimization of crop productivity in tomato using induced mutations in the florigen pathway. *Nat. Genet.* **46**, 1337–42 (2014).
12. Hamada, S. et al. The transport of prolamine RNAs to prolamine protein bodies in living rice endosperm cells. *Plant Cell* **15**, 2253–2264 (2003).
13. Zhang, F. Simon, A. E. A novel procedure for the localization of viral RNAs in protoplasts and whole plants. *Plant J.* **35**, 665–673 (2003).
14. Schönberger, J., Hammes, U. Z. & Dresselhaus, T. In vivo visualization of RNA in plants cells using the λN_{22} system and a GATEWAY-compatible vector series for candidate RNAs. *Plant J.* **71**, 173–181 (2012).
15. Lenstra, T. L., Rodriguez, J., Chen, H. & Larson, D. R. Transcription dynamics in living cells. *Annu. Rev. Biophys.* **45**, 25–47 (2016).
16. Larson, D. R., Zenklusen, D., Wu, B., Chao, J. A. & Singer, R. H. Real-time observation of transcription initiation and elongation on an endogenous yeast gene. *Science* **332**, 475–478 (2011).
17. Lammers, N. C. et al. Multimodal transcriptional control of pattern formation in embryonic development. *Proc. Natl Acad. Sci. USA* **117**, 836–847 (2020).
18. Bindels, D. S. et al. mScarlet : a bright monomeric red fluorescent protein for cellular imaging. *Nat. Methods* **14**, 53–56 (2016).
19. Mittler, R., Finka, A. & Goloubinoff, P. How do plants feel the heat? *Trends Biochem. Sci.* **37**, 118–125 (2012).
20. Czechowski, T., Stitt, M., Altmann, T., Udvardi, M. K. & Scheible, W.-R. Genome-wide identification and testing of superior reference genes for transcript normalization in *Arabidopsis*. *Plant Physiol.* **139**, 5–17 (2005).
21. Sung, D. Y., Vierling, E. & Guy, C. L. Comprehensive expression profile analysis of the *Arabidopsis hsp70* gene family. *Plant Physiol.* **126**, 789–800 (2001).
22. Hocine, S., Raymond, P., Zenklusen, D., Chao, J. A. & Singer, R. H. Single-molecule analysis of gene expression using two-color RNA labeling in live yeast. *Nat. Methods* **10**, 119–121 (2012).
23. Coulon, A. et al. Kinetic competition during the transcription cycle results in stochastic rna processing. *eLife* **3**, e03939 (2014).
24. Fukaya, T., Lim, B. & Levine, M. Enhancer control of transcriptional bursting. *Cell* **166**, 358–368 (2016).
25. Bertrand, E. et al. Localization of ASH1 mRNA particles in living yeast. *Mol. Cell* **2**, 437–445 (1998).

26. Liu, M., Zhu, J. & Dong, Z. Immediate transcriptional responses of *Arabidopsis* leaves to heat shock. *Plant Biol.* **63**, 468–483 (2020).
27. Winter, D. et al. An 'electronic fluorescent pictograph' browser for exploring and analyzing large-scale biological data sets. *PLoS ONE* **2**, 0000718 (2007).
28. Hsia, Y. et al. Design of a hyperstable 60-subunit protein icosahedron. *Nature* **535**, 136–139 (2016).
29. Akamatsu, M. et al. Principles of self-organization and load adaptation by the actin cytoskeleton during clathrin-mediated endocytosis. *eLife* **9**, e49840 (2020).
30. Delarue, M. et al. mTORC1 controls phase separation and the biophysical properties of the cytoplasm by tuning crowding. *Cell* **174**, 338–349 (2018).
31. Ardehali, M. B. & Lis, J. T. Tracking rates of transcription and splicing in vivo. *Nat. Struct. Mol. Biol.* **16**, 1123–1124 (2009).
32. The *Arabidopsis* Genome Iniative. Analysis of the genome sequence of the flowering plant *Arabidopsis thaliana*. *Nature* **408**, 796–815 (2000).
33. Tornaletti, S., Reines, D. & Hanawalt, P. C. Structural characterization of RNA polymerase II complexes arrested by a cyclobutane pyrimidine dimer in the transcribed strand of template DNA. *J. Biol. Chem.* **274**, 24124–24130 (1999).
34. Birnbaum, K. D. Power in numbers: single-cell RNA-seq strategies to dissect complex tissues. *Annu. Rev. Genet.* **52**, 203–221 (2018).
35. Melaragno, J. E., Mehrotra, B. & Coleman, A. W. Relationship between endopolyploidy and cell size in epidermal tissue of *Arabidopsis*. *Plant Cell* **5**, 1661–1668 (1993).
36. Robinson, D. O. et al. Ploidy and size at multiple scales in the *Arabidopsis* sepal. *Plant Cell* **30**, 2308–2329 (2018).
37. Queitsch, C., Hong, S. W., Vierling, E. & Lindquist, S. Heat shock protein 101 plays a crucial role in thermotolerance in *Arabidopsis*. *Plant Cell* **12**, 479–492 (2000).
38. Charng, Y.-Y. et al. A heat-inducible transcription factor, HsfA2 is required for extension of acquired thermotolerance. *Plant Physiol.* **143**, 251–262 (2007).
39. Hafner, A. et al. Quantifying the central dogma in the p53 pathway in live single cells. *Cell Syst.* **10**, 495–505 (2020).
40. McLoughlin, F. et al. Class I and II small heat shock proteins together with HSP101 protect protein translation factors during heat stress. *Plant Physiol.* **172**, 1221–1236 (2016).
41. Nicolas, D., Phillips, N. E. & Naef, F. What shapes eukaryotic transcriptional bursting? *Mol. BioSyst.* **13**, 1280–1290 (2017).
42. Ietswaart, R., Rosa, S., Wu, Z., Dean, C. & Howard, M. Cell-size-dependent transcription of FLC and its antisense long non-coding RNA COOLAIR explain cell-to-cell expression variation. *Cell Syst.* **4**, 622–635 (2017).
43. Shermoen, A. W. & Farrell, P. H. O. Progression of the cell cycle through mitosis leads to abortion of nascent transcripts. *Cell* **67**, 303–310 (1991).
44. Ko, M. S. H. Induction mechanism of a single molecule: stochastic or deterministic? *BioEssays* **14**, 341–346 (1992).
45. Fiering, S., Whitelaw, E. & Martin, D. I. K. To be or not to be active: the stochastic nature of enhancer action. *BioEssays* **22**, 381–387 (2000).
46. Turco, G. M. et al. Molecular mechanisms driving switch behavior in xylem cell differentiation. *Cell Rep.* **28**, 342–351.e4 (2019).
47. Angel, A., Song, J., Dean, C. & Howard, M. A Polycomb-based switch underlying quantitative epigenetic memory. *Nature* **476**, 105–109 (2011).
48. Raj, A. & van Oudenaarden, A. Nature, nurture, or chance: stochastic gene expression and its consequences. *Cell* **135**, 216–226 (2008).
49. Cortijo, S. & Locke, J. C. W. Does gene expression noise play a functional role in plants? *Trends Plant Sci.* **25**, 1041–1051 (2020).
50. Meyer, H. M. et al. Fluctuations of the transcription factor ATML1 generate the pattern of giant cells in the *Arabidopsis* sepal. *eLife* **6**, e19131 (2017).
51. Stapel, L. C., Zechner, C. & Vastenhouw, N. L. Uniform gene expression in embryos is achieved by temporal averaging of transcription noise. *Genes Dev.* **31**, 1635–1640 (2017).
52. Raj, A., Peskin, C. S., Tranchina, D., Vargas, D. Y. & Tyagi, S. Stochastic mRNA synthesis in mammalian cells. *PLoS Biol* **4**, e309 (2006).
53. Battich, N., Stoeger, T. & Pelkmans, L. Control of transcript variability in single mammalian cells. *Cell* **163**, 1596–1610 (2015).
54. Raser, J. M. & O'Shea, E. K. Control of stochasticity in eukaryotic gene expression. *Science* **304**, 1811–1814 (2004).
55. Yang, S. et al. Contribution of RNA polymerase concentration variation to protein expression noise. *Nat. Commun.* **5**, 4761 (2014).
56. Elowitz, M. B., Levine, A. J., Siggia, E. D. & Swain, P. S. Stochastic gene expression in a single cell. *Science* **297**, 1183–1186 (2002).
57. Araújo, I. S. et al. Stochastic gene expression in *Arabidopsis thaliana*. *Nat. Commun.* **8**, 2132 (2017).
58. Jupe, F. et al. The complex architecture and epigenomic impact of plant T-DNA insertions. *PLoS Genet.* **15**, e1007819 (2019).
59. McFaline-Figueroa, J. L., Trapnell, C. & Cuperus, J. T. The promise of single-cell genomics in plants. *Curr. Op. Plant Biol.* **54**, 114–121 (2020).
60. Duncan, S., Olsson, T. S. G., Hartley, M., Dean, C. & Rosa, S. A method for detecting single mRNA molecules in *Arabidopsis thaliana*. *Plant Methods* **12**, 13 (2016).
61. Rodriguez, J. et al. Intrinsic dynamics of a human gene reveal the basis of expression heterogeneity. *Cell* **176**, 213–226 (2019).
62. Cortijo, S. et al. Transcriptional regulation of the ambient temperature response by H2A.Z nucleosomes and HSF1 transcription factors in *Arabidopsis*. *Mol. Plant* **10**, 1258–1273 (2017).
63. Novick, A. & Weiner, M. Enzyme induction as an all-or-none phenomenon. *Proc. Natl Acad. Sci. USA* **43**, 553–566 (1957).
64. Little, S. C., Tikhonov, M. & Gregor, T. Precise developmental gene expression arises from globally stochastic transcriptional activity. *Cell* **154**, 789–800 (2013).
65. Li, Z. et al. Gene duplicability of core genes is highly consistent across all angiosperms. *Plant Cell* **28**, 326–344 (2015).
66. Liu, T. L. et al. Observing the cell in its native state: Imaging subcellular dynamics in multicellular organisms. *Science* **360**, eaaq1392 (2018).
67. Wu, Z. et al. Quantitative regulation of FLC via coordinated transcriptional initiation and elongation. *Proc. Natl Acad. Sci. USA* **113**, 218–223 (2016).
68. Tantale, K. et al. A single-molecule view of transcription reveals convoys of RNA polymerases and multi-scale bursting. *Nat. Commun.* **7**, 12248 (2016).
69. Iwatate, R. et al. Covalent self-labeling of tagged proteins with chemical fluorescent dyes in BY-2 cells and *Arabidopsis* seedlings. *Plant Cell* **32**, 3081–3094 (2020).
70. Wu, D. et al. Structural basis of ultraviolet-B perception by UVR8. *Nature* **484**, 214–219 (2012).
71. Daigle, N. & Ellenberg, J. λ_N-GFP: an RNA reporter system for live-cell imaging. *Nat. Methods* **4**, 633–636 (2007).
72. Ronald, J. & Davis, S. J. Focusing on the nuclear and subnuclear dynamics of light and circadian signalling. *Plant Cell Environ.* **42**, 2871–2884 (2019).
73. Phillips, R. et al. Figure 1 theory meets Figure 2 experiments in the study of gene expression. *Annu. Rev. Biophys.* **48**, 121–163 (2019).
74. Yoshida, T. et al. *Arabidopsis HsfA1* transcription factors function as the main positive regulators in heat shock-responsive gene expression. *Mol. Genet. Genomics* **286**, 321–332 (2011).
75. Liu, H., Liu, B., Zhao, C., Pepper, M. & Lin, C. The action mechanisms of plant cryptochromes. *Trends Plant Sci* **16**, 684–691 (2011).
76. Arganda-Carreras, I. et al. Trainable weka segmentation: a machine learning tool for microscopy pixel classification. *Bioinformatics* **33**, 2424–2426 (2017).

Acknowledgements

We thank R. Phillips, A. Roeder, P. Quail, S. Wakao, C. Gee, J. Brunkard and A. Flamholz for comments on the manuscript; members of the Garcia laboratory: M. Turner and G. Martini for sharing their knowledge and materials related to the nanocages experiment and Y. J. Kim for discussing results, G. Martini in particular for setting up the microscope temperature chamber; C. Baker, S. Wakao and D. Westcott from the Niyogi laboratory for their RT–qPCR advice; A. Schwartz, J. O'Brien and F. Federici for sharing plasmids; A. Lin and J. Liu provided useful feedback regarding calculations; and M. Kobayashi for help and for making the Niyogi laboratory run smoothly. H.G.G. was supported by the Burroughs Wellcome Fund Career Award at the Scientific Interface, the Sloan Research Foundation, the Human Frontiers Science Program, the Searle Scholars Program, the Shurl and Kay Curci Foundation, the Hellman Foundation, the National Institutes for Health Director's New Innovator Award (DP2 OD024541-01), and a National Science Foundation CAREER Award (1652236). K.K.N. is an investigator of the Howard Hughes Medical Institute. S.A. was supported by H.G.G. and K.K.N. A.R. was supported by H.G. and National Science Foundation Graduate Research Fellowships Program (DGE 1752814).

Author contributions

S.A., H.G.G. and K.K.N. designed experiments. S.A. performed experiments and analysed the data. S.A., A.R. and H.G.G. wrote the analysis code. S.A., H.G.G. and K.K.N. wrote the paper.

Competing interests

The authors declare no competing interests.

Additional information

Supplementary information The online version contains supplementary material available at https://doi.org/10.1038/s41477-021-00976-0.

Correspondence and requests for materials should be addressed to K.K.N. or H.G.G.

Peer review information *Nature Plants* thanks Zhicheng Dong and the other, anonymous, reviewer(s) for their contribution to the peer review of this work.

Reprints and permissions information is available at www.nature.com/reprints.

Publisher's note Springer Nature remains neutral with regard to jurisdictional claims in published maps and institutional affiliations.

nature research

Corresponding author(s): Hernan Garcia and Krishna Niyogi

Last updated by author(s): Oct 28, 2020

Reporting Summary

Nature Research wishes to improve the reproducibility of the work that we publish. This form provides structure for consistency and transparency in reporting. For further information on Nature Research policies, see our Editorial Policies and the Editorial Policy Checklist.

Statistics

For all statistical analyses, confirm that the following items are present in the figure legend, table legend, main text, or Methods section.

n/a	Confirmed
☐	☒ The exact sample size (*n*) for each experimental group/condition, given as a discrete number and unit of measurement
☐	☒ A statement on whether measurements were taken from distinct samples or whether the same sample was measured repeatedly
☐	☒ The statistical test(s) used AND whether they are one- or two-sided *Only common tests should be described solely by name; describe more complex techniques in the Methods section.*
☒	☐ A description of all covariates tested
☒	☐ A description of any assumptions or corrections, such as tests of normality and adjustment for multiple comparisons
☐	☒ A full description of the statistical parameters including central tendency (e.g. means) or other basic estimates (e.g. regression coefficient) AND variation (e.g. standard deviation) or associated estimates of uncertainty (e.g. confidence intervals)
☐	☒ For null hypothesis testing, the test statistic (e.g. *F*, *t*, *r*) with confidence intervals, effect sizes, degrees of freedom and *P* value noted *Give P values as exact values whenever suitable.*
☒	☐ For Bayesian analysis, information on the choice of priors and Markov chain Monte Carlo settings
☒	☐ For hierarchical and complex designs, identification of the appropriate level for tests and full reporting of outcomes
☒	☐ Estimates of effect sizes (e.g. Cohen's *d*, Pearson's *r*), indicating how they were calculated

Our web collection on statistics for biologists contains articles on many of the points above.

Software and code

Policy information about availability of computer code

Data collection	We used the Leica LASX microscope controller software for image acquisition and the Applied Biosystems 7500 FAST software version 2.0.4 for qPCR data collection.
Data analysis	We used Matlab version 2020a and imageJ2. Our code is publicly available from github at https://github.com/GarciaLab/mRNADynamics and https://github.com/GarciaLab/PlantPP7.

For manuscripts utilizing custom algorithms or software that are central to the research but not yet described in published literature, software must be made available to editors and reviewers. We strongly encourage code deposition in a community repository (e.g. GitHub). See the Nature Research guidelines for submitting code & software for further information.

Data

Policy information about availability of data

All manuscripts must include a data availability statement. This statement should provide the following information, where applicable:

- Accession codes, unique identifiers, or web links for publicly available datasets
- A list of figures that have associated raw data
- A description of any restrictions on data availability

The datasets generated during the current study are available from the corresponding author upon reasonable request.

Field-specific reporting

Please select the one below that is the best fit for your research. If you are not sure, read the appropriate sections before making your selection.

☒ Life sciences ☐ Behavioural & social sciences ☐ Ecological, evolutionary & environmental sciences

For a reference copy of the document with all sections, see nature.com/documents/nr-reporting-summary-flat.pdf

Life sciences study design

All studies must disclose on these points even when the disclosure is negative.

Sample size	Between 3 and 8 samples (movies taken from different individuals of the same genotype) were used to obtain statistics in all experiments showing means and standard deviations, except for the intrinsic/extrinsic noise analysis. We found that the variability across individuals was low enough that a sample size of three can capture the mean and the standard error reasonably well. In the case of the noise analysis we decided to analyze three different genotypes instead of multiple replicates of the same genotype. We did this to determine if there were qualitative aspects that were consistent across different genotypes. In this case, in order to estimate the confidence of our measurements we bootstrapped the standard error and the mean of each genotype.
Data exclusions	No data was excluded.
Replication	We found the experiments to be qualitatively reproducible. The degree of quantitative reproducibility is shown in the figures.
Randomization	Plants of a given genotype were selected at random.
Blinding	Blinding was not relevant to this study since data analysis was done largely computationally applying the same algorithm consistently across samples.

Reporting for specific materials, systems and methods

We require information from authors about some types of materials, experimental systems and methods used in many studies. Here, indicate whether each material, system or method listed is relevant to your study. If you are not sure if a list item applies to your research, read the appropriate section before selecting a response.

Materials & experimental systems

n/a	Involved in the study
☒	☐ Antibodies
☒	☐ Eukaryotic cell lines
☒	☐ Palaeontology and archaeology
☐	☒ Animals and other organisms
☒	☐ Human research participants
☒	☐ Clinical data
☒	☐ Dual use research of concern

Methods

n/a	Involved in the study
☒	☐ ChIP-seq
☒	☐ Flow cytometry
☒	☐ MRI-based neuroimaging

Animals and other organisms

Policy information about studies involving animals; ARRIVE guidelines recommended for reporting animal research

Laboratory animals	no animals were used in this study.
Wild animals	no animals were used in this study.
Field-collected samples	no animals were used in this study.
Ethics oversight	no animals were used in this study.

Note that full information on the approval of the study protocol must also be provided in the manuscript.